

## Ultrafast Carrier Dynamics in Graphite

Markus Breusing,<sup>1</sup> Claus Ropers,<sup>1,2,\*</sup> and Thomas Elsaesser<sup>1</sup><sup>1</sup>Max-Born-Institut für Nichtlineare Optik und Kurzzeitspektroskopie, D-12489 Berlin, Germany<sup>2</sup>Courant Research Center Nano-Spectroscopy and X-Ray Imaging, University of Göttingen, Germany

(Received 5 September 2008; published 27 February 2009)

Optical pump-probe spectroscopy with 7-fs pump pulses and a probe spectrum wider than 0.7 eV reveals the ultrafast carrier dynamics in freestanding thin graphite films. We discern for the first time a rapid intraband carrier equilibration within 30 fs, leaving the system with separated electron and hole chemical potentials. Phonon-mediated intraband cooling of electrons and holes occurs on a 100 fs time scale. The kinetics are in agreement with simulations based on Boltzmann equations.

DOI: 10.1103/PhysRevLett.102.086809

PACS numbers: 81.05.Uw, 63.20.kd, 78.47.J-, 78.40.Kc

Individual carbon layers with hexagonal symmetry define the structure of graphite and graphene. Graphite forms a crystal structure consisting of a stack of such layers, while the quasi-two-dimensional graphene consists of a single layer. These materials possess unique electronic and lattice properties that are of high current interest both from the viewpoint of basic physics, and for applications in carbon-based electronics [1,2]. At the  $K$  point in reciprocal space, the electronic band structure of both materials displays a vanishing energy gap between the valence and conduction bands with—for a single layer—identical linear  $k$  dispersions of the two bands [3].

The dynamics of elementary excitations in graphite and graphene occur on ultrafast time scales, governed by the interaction among carriers and their coupling to the lattice [4–12]. Despite substantial progress, the carrier dynamics are not fully understood. Optical interband excitation [Fig. 1(a)] by an ultrashort optical pulse generates a non-equilibrium carrier distribution defined by excess electrons in the conduction band and holes in the valence band. This athermal distribution transforms into a quasiequilibrium distribution by carrier-carrier (cc) and carrier-phonon scattering. There are two potential scenarios for this equilibration process: (i) For similar rates of intra- and interband scattering of carriers, a hot equilibrium (Fermi) distribution with a chemical potential  $\mu = 0$ , an elevated carrier temperature and, thus, a strong variation of the conduction band population is formed [Fig. 1(b)]. Formation of this distribution involves ultrafast electron-hole recombination processes. On a somewhat longer time scale, carriers cool down by carrier-phonon scattering. (ii) For intraband scattering rates much higher than interband scattering/recombination, intraband equilibration at persistent electron and hole densities establishes separate Fermi distributions of electrons in the conduction and holes in the valence band. These *quasiequilibrium* distributions are characterized by separate nonzero chemical potentials and elevated temperatures  $T_e$  and  $T_h$  of electrons and holes, which vary in time during the phonon-mediated carrier cooling [Fig. 1(c)]. For the symmetric band structure of Fig. 1(a)

and similar cooling rates of electrons and holes,  $T_e$  and  $T_h$  are identical at all times. Eventually, interband scattering including electron-hole recombination establishes a single *equilibrium* distribution with  $\mu = 0$ . Existing theoretical and experimental work has left this issue unresolved, which touches on the fundamental question if ultrafast carrier dynamics in the semimetal graphite [13,14] resem-

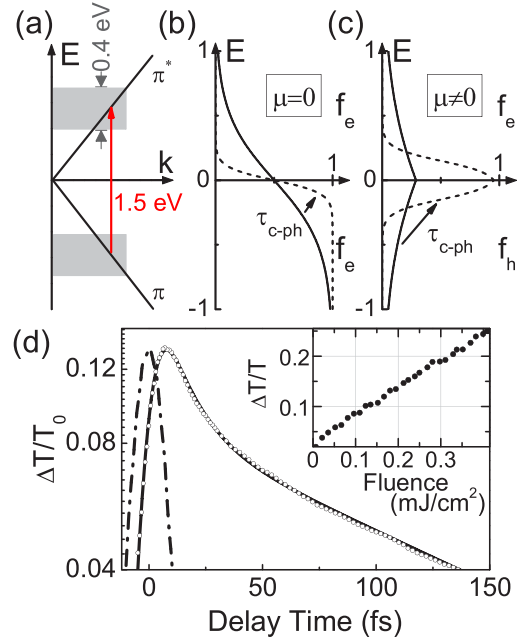


FIG. 1 (color online). (a) Idealized linear band structure of graphene, red arrow indicating pumped and probed direct optical transitions. (b) Schematic of temporally evolving electronic occupation probabilities after optical excitation and under the influence of carrier-phonon scattering (indicated by  $\tau_{c-ph}$ ), assuming a thermalization towards zero chemical potential. (c) The same for persistent carrier densities ( $\mu \neq 0$ ). (d) Spectrally integrated DT as a function of pump-probe delay: experiment (open circles) and numerical fit (solid line). Dash-dotted line: Cross correlation of pump and probe pulses. Inset: Linear dependence of the maximum transmission change on the absorbed pump fluence.

bles more closely that of a metal [Fig. 1(b)] or a semiconductor [Fig. 1(c)].

Carrier-optical phonon (cop) coupling is important for carrier equilibration, cooling, and recombination. Theoretical studies have predicted cop scattering times of few tens of femtoseconds and the generation of pronounced transient nonequilibrium populations of optical phonons [8]. Such phonon excess populations decelerate carrier cooling, and may limit ballistic transport in graphene [15]. Experimental work on ultrafast carrier dynamics in graphite and graphene has led to conflicting results. Early pump-probe studies of graphite of about 50 fs resolution have been interpreted in terms of an “instantaneous” equilibration, followed by electron cooling on a 100 fs time scale [4]. In contrast, a time-resolved photoemission experiment has claimed an electron equilibration time of  $250 \pm 50$  fs and a 2 ps time scale for electron cooling [6]. Recent studies of the response of graphite at THz frequencies indicate that the electronic system has lost 90% of the excess energy after 500 fs [7].

Optical experiments with a temporal resolution significantly shorter than the relevant relaxation times are required to characterize the transient carrier distributions and their time evolution. In this Letter, we present an optical pump-probe study of carrier dynamics in freestanding graphite films with a time resolution of about 10 fs. Mapping carrier populations over an energy range of 0.6 eV, we observe an ultrafast intraband equilibration within 20–30 fs, leading to separate electron and hole distributions in the conduction and valence bands. Carrier cooling occurs on a 100 fs scale, followed by electron-hole recombination on a picosecond time scale.

In our experiments, we investigated 20–30 nm thick flakes of highly oriented pyrolytic graphite (HOPG) peeled off a substrate with a mosaicity of  $0.4^\circ$  by adhesive tape. After removal of the tape and cleaning, the films are mounted on a fine metallic mesh and show freestanding areas of homogeneous thickness, several tens of micrometers in diameter. Optical characterization indicates that the graphite structure remains intact in the sample preparation. Time-resolved measurements with different graphite samples give identical results. Orthogonally polarized 7-fs pump and probe pulses are noncollinearly focused onto the sample to a spot size of about  $5 \times 5 \mu\text{m}^2$  using a mirror objective for minimal spectral dispersion. The pump beam is modulated with a mechanical chopper. The transmitted (and reflected) probe pulses are spectrally dispersed in a grating monochromator and detected with a photodiode in conjunction with a lock-in amplifier. The time resolution derived from the pump-probe cross correlation [Fig. 1(d)] is approximately 10 fs.

The pump-induced change of transmission is dominated by absorption saturation of direct optical transitions [Fig. 1(a)], resulting in a positive differential transmission (DT)  $\Delta T/T_0 = (T - T_0)/T_0$ ;  $T$  and  $T_0$  are sample transmissions with and without excitation, respectively. In Fig. 1(d), the spectrally integrated DT is plotted on a

logarithmic scale as a function of delay time. The very high time resolution of the experiment allows for discerning an ultrafast initial decay which has not been observed so far and is followed by a slower decrease of DT. A numerical fit convoluted with the cross correlation gives time constants  $\tau_1 = 13 \pm 3$  fs and  $\tau_2 \approx 100$  fs for the two components (solid line). The DT peak signal scales linearly with the absorbed pump fluence [inset of Fig. 1(d)].

In Fig. 2(a), the DT is presented as a function of delay time (abscissa) and probe photon energy  $E_{\text{pr}}$  (absorbed fluence  $0.36 \text{ mJ/cm}^2$ , corresponding to an excitation density  $5 \times 10^{20} \text{ cm}^{-3}$ ). The ordinate scale on the right-hand side gives the energy of the carriers  $E_{e,h} = E_{\text{pr}}/2$  probed at  $E_{\text{pr}}$  [cf. Fig. 1(a)]. Time traces for fixed photon energies  $E_{\text{pr}}$  [Fig. 2(b)] display a predominant decay with  $\tau_2 \approx 50$ –250 fs and a slower picosecond component, both depending on  $E_{\text{pr}}$  [inset of Fig. 2(b)]. The amplitude of the initial 15 fs component [cf. Fig. 1(d)] is minor. At time delays beyond 100 fs and photon energies  $E_{\text{pr}} > 1.3$  eV, the signal develops a negative amplitude [4,12]. Transient DT spectra for fixed time delays are summarized in Fig. 3 (solid black lines). Even for time delays as short as 20 fs, the DT signal decreases monotonically towards higher photon energies  $E_{\text{pr}}$ , i.e., does not reflect the pump spectrum (top panel).

We now discuss the processes underlying the ultrafast optical response. The DT signals of positive sign are due to transient populations in the optically coupled states that block the corresponding interband transitions (state filling). In contrast, negative DT signals reflect band-gap

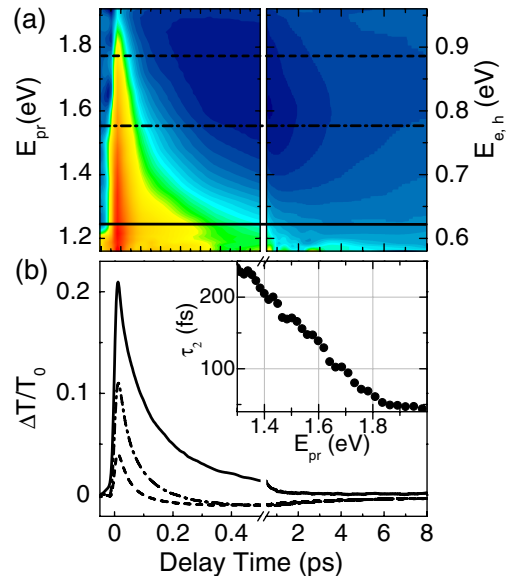


FIG. 2 (color online). (a) Spectrally resolved differential transmission (DT) plotted as a function of probe photon energy  $E_{\text{pr}}$  and short and long pump-probe delays (excitation density  $5 \times 10^{20} \text{ cm}^{-3}$ ). (b) DT transients at  $E_{\text{pr}} = 1.24$  eV (solid), 1.55 eV (dash-dotted) and 1.77 eV (dashed) for short and long delays. Inset: Decay time  $\tau_2$  vs  $E_{\text{pr}}$ .

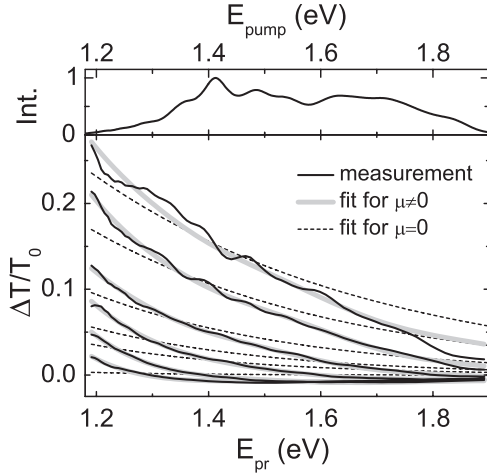


FIG. 3. Top: Optical pump spectrum. Bottom: Experimental DT spectra (solid black lines) for fixed time delays of (top to bottom) 20, 40, 80, 150, 250, and 1000 fs, together with fits to the model described in the text (gray lines) and best-fit DT spectra assuming a zero chemical potential (dashed lines).

renormalization by the photogenerated electron-hole plasma, leading to a redshift of interband absorption [16]. The biphasic decay of the spectrally integrated signal [Fig. 1(d)] is due to the depopulation of the optically coupled valence and conduction band states by scattering of carriers into lower and higher lying continuum states. Here, both cc and cop scattering contribute. The high excitation density in our experiments results in very high intraband cc scattering rates, spreading electrons and holes over a wide energy range. The fast 13 fs decay mainly reflects this process, establishing hot quasiequilibrium distributions within 20 to 30 fs. The optically coupled window is located on the high-energy tail of such distributions, some 0.7 eV above and below the  $K$  point. Thus, also carrier cooling by cop scattering leads to a decrease of the positive DT on a slower 100 fs time scale. This picture is confirmed by the spectrally resolved data: the shape of the transient spectrum for a 20 fs delay time is very close to the behavior expected for quasiequilibrium distributions at high temperature. The changes in amplitude and slope of the spectra at later delay times nicely reflect carrier cooling. The variation of decay times with photon energy [Fig. 2(b)] is fully in line with cooling of quasiequilibrium distributions in which states well up on the high-energy tail undergo a faster depopulation than lower lying states.

To extract quantitative information, we calculated DT spectra for quasiequilibrium carrier distributions and fitted them to the measured spectra. Because of the symmetric conical band structure [cf. Fig. 1(a), [3]], electrons and holes behave in equivalent ways [ $f_e(E) = f_h(-E)$ ], and the change in the imaginary part of the dielectric function is

$$\Delta \underline{\varepsilon} = \underline{\varepsilon}(E + dE) - \underline{\varepsilon}(E) - 2\underline{\varepsilon}(E + dE)f_e\left(\frac{E + dE}{2}\right).$$

Here,  $\underline{\varepsilon}(E)$  is the imaginary part of the dielectric function at the photon energy  $E$  [17],  $dE$  is the shift from band-gap renormalization (left as a free parameter), and the argument in the electron distribution  $f_e$  corresponds to the single particle energies in the two bands. The DT is calculated from  $\Delta \underline{\varepsilon}$  using Fresnel's equations [18].

In Fig. 3, we present spectra calculated with separate Fermi-Dirac distributions  $f_{e,h}(E) = (1 + \exp[(\pm E \mp \mu_{e,h})/T_{e,h}])^{-1}$  of electrons and holes [solid gray lines, cf. Fig. 1(c)] and for a chemical potential  $\mu = 0$ , i.e., a single Fermi-Dirac distribution of electrons [dashed lines, cf. Fig. 1(b)]. The former approach is in excellent agreement with our data for all time delays. The time-dependent carrier temperatures  $T_e = T_h$  and chemical potentials  $\mu_e = -\mu_h$  of electrons and holes extracted are plotted in Fig. 4(a). The carrier temperature decreases from its initial value of about 2500 K to less than 1000 K within the first 200 fs. The calculations suggest a renormalization of the band gap by  $dE \approx 30$  meV which is nearly constant during the first picosecond.

The transient spectra calculated with a single Fermi distribution ( $\mu = 0$ ) are in disagreement with the experiment. The slope of such best-fit DT spectra towards higher photon energies is much smaller than in the data. For  $\mu = 0$ , the optically coupled window probes the tail of the electron distribution at higher energies than for  $\mu \neq 0$  and, thus, the slope of the Fermi function and the spectra is smaller. We conclude that, similar to semiconductors with a nonzero band gap, carrier equilibration in graphite

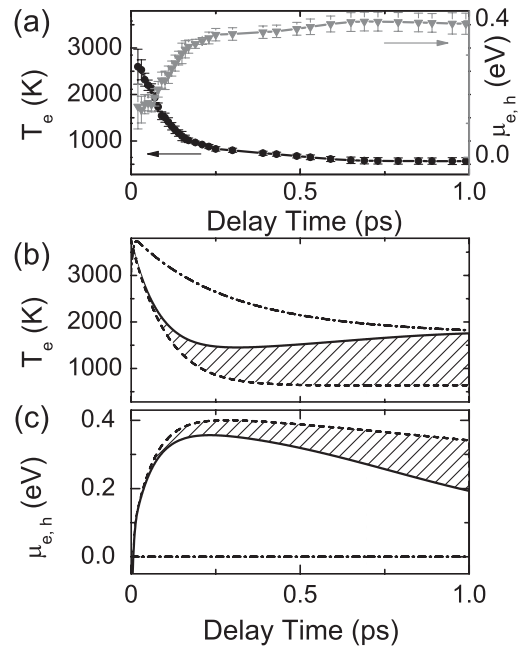


FIG. 4. (a) Time-dependent carrier temperature (black circles) and chemical potential (gray triangles) derived from the fit to the data of Figs. 2 and 3. (b) Carrier temperature and (c) chemical potential calculated with instantaneous (dashed lines) and without (solid lines) phonon decay; dash-dotted lines represent a simulation with  $\mu = 0$ .



establishes separate quasiequilibrium distributions of electrons and holes that cool down on a femtosecond time scale. This is followed by electron-hole recombination in the picosecond regime, leading to a (single) equilibrium distribution with  $\mu = 0$ . Recombination gives rise to the picosecond decay of DT in Fig. 2, similar to what has been reported in Refs. [11,12].

For an analysis of the microscopic scattering processes, we simulated carrier dynamics by solving the Bloch-Boltzmann-Peierls (BBP) equations [19]. Angularly averaged cop coupling constants and optical phonon frequencies of graphite were taken from Refs. [20–22]. To reduce numerical efforts, only the electronic band structure in the layer plane is considered, motivated by the small interlayer coupling in graphite. The band structure is treated as two-dimensional, conical and symmetric about the initial  $\mu = 0$ . The electron distribution is assumed to be isotropic, a simplification justified in light of the ultrafast thermalization found here. A recent measurement of optical phonon dephasing times in graphite [10] set a lower limit to the optical phonon lifetime  $\tau_{\text{ph}} > 500$  fs, while THz measurements suggest  $\tau_{\text{ph}} \leq 7$  ps [7]. We present calculations for both  $\tau_{\text{ph}} \rightarrow \infty$  and  $\tau_{\text{ph}} = 0$ , in the latter case fully suppressing hot phonon effects [8]. Finally, carrier equilibration is included in a relaxation time approximation with a 20 fs time constant.

In the simulation, the carrier source term in the BBP equations is entered according to the temporal and spectral pump pulse profiles in the experiment. After carrier equilibration within the first 20–30 fs, one obtains the transient temperatures and chemical potentials shown in Figs. 4(b) and 4(c) for separate electron and hole distributions vs a single electron distribution (including recombination terms). The first model fully reproduces the initial value and the fast decrease of carrier temperature found in the experiments. Hot phonon effects are negligible at such early times, but may come into play after approximately 100 fs. The shaded regions between the curves for zero (dashed) and infinite (solid)  $\tau_{\text{ph}}$  represent the range of  $T_e$  and  $\mu$  values resulting for finite optical phonon lifetimes. The experimental values are closer to the lower boundary in Fig. 4(b) which points to a limited role of energy back-transfer from the lattice into the carrier system. The calculation with a single electron distribution does not account for our data, as is evident from the much slower decrease of carrier temperature and the—by definition—constant chemical potential. Our analysis suggests a slowing down of interband cc and cop scattering by density of states effects and Pauli blocking, in line with the observed picosecond recombination kinetics.

In conclusion, ultrafast pump-probe experiments with a 10 fs time resolution, in combination with theoretical calculations, demonstrate intraband carrier equilibration

in optically excited graphite within 20–30 fs, and strongly suggest the evolution of separate electron and hole distributions. Our results indicate semiconductorlike carrier dynamics even for excitation densities on the order of  $10^{20}$  cm<sup>-3</sup>. The hot quasiequilibrium carriers lose a major fraction of their excess energy within 200 fs, mainly by emission of optical phonons. On this time scale, hot phonon effects play a minor role. Electron-hole recombination establishes an electron distribution with a chemical potential  $\mu = 0$  in the slower picosecond regime.

We thank M. Tischer for sample preparation and H. Petek, F. Milde, and T. Kampfrath for useful discussions.

---

\*croppers@gwdg.de

- [1] A. K. Geim and K. S. Novoselov, *Nature Mater.* **6**, 183 (2007).
- [2] P. Avouris, Z. Chen, and V. Perebeinos, *Nature Nanotech.* **2**, 605 (2007).
- [3] P. R. Wallace, *Phys. Rev.* **71**, 622 (1947).
- [4] K. Seibert *et al.*, *Phys. Rev. B* **42**, 2842 (1990).
- [5] S. Xu *et al.*, *Phys. Rev. Lett.* **76**, 483 (1996).
- [6] G. Moos, C. Gahl, R. Fasel, M. Wolf, and T. Hertel, *Phys. Rev. Lett.* **87**, 267402 (2001).
- [7] T. Kampfrath, L. Perfetti, F. Schapper, C. Frischkorn, and M. Wolf, *Phys. Rev. Lett.* **95**, 187403 (2005).
- [8] S. Butscher, F. Milde, M. Hirtschulz, E. Malić, and A. Knorr, *Appl. Phys. Lett.* **91**, 203103 (2007).
- [9] A. Bostwick, T. Ohta, T. Seyller, K. Horn, and E. Rotenberg, *Nature Phys.* **3**, 36 (2007).
- [10] K. Ishioka *et al.*, *Phys. Rev. B* **77**, 121402(R) (2008).
- [11] J. M. Dawlaty, S. Shivaraman, M. V. S. Chandrashekar, F. Rana, and M. G. Spencer, *Appl. Phys. Lett.* **92**, 042116 (2008).
- [12] D. Sun *et al.*, *Phys. Rev. Lett.* **101**, 157402 (2008).
- [13] A. Santoni, L. J. Terminello, F. J. Himpsel, and T. Takahashi, *Appl. Phys. A* **52**, 299 (1991).
- [14] A. Zunger, *Phys. Rev. B* **17**, 626 (1978).
- [15] M. Lazzeri, S. Piscanec, F. Mauri, A. C. Ferrari, and J. Robertson, *Phys. Rev. Lett.* **95**, 236802 (2005).
- [16] H. Haug and S. Koch, *Quantum Theory of the Optical and Electronic Properties of Semiconductors* (World Scientific Publishing, Singapore, 2004).
- [17] D. W. Lynch and W. R. Hunter, *Handbook of Optical Constants of Solids*, edited by E. D. Palik (Academic Press, San Diego, 1998).
- [18] The real part of the dielectric function has negligible influence on the DT.
- [19] J. M. Ziman, *Electrons and Phonons* (Oxford University Press, New York, 2001).
- [20] S. Piscanec, M. Lazzeri, F. Mauri, A. C. Ferrari, and J. Robertson, *Phys. Rev. Lett.* **93**, 185503 (2004).
- [21] M. Lazzeri, S. Piscanec, F. Mauri, A. C. Ferrari, and J. Robertson, *Phys. Rev. B* **73**, 155426 (2006).
- [22] J. Maultzsch, S. Reich, C. Thomsen, H. Requardt, and P. Ordejón, *Phys. Rev. Lett.* **92**, 075501 (2004).